APL Materials

Efficient suboxide sources in oxide molecular beam epitaxy using mixed metal + oxide charges: The examples of SnO and Ga_2O

Cite as: APL Mater. 8, 031110 (2020); https://doi.org/10.1063/1.5134444
Submitted: 30 October 2019 . Accepted: 21 February 2020 . Published Online: 12 March 2020

Georg Hoffmann, Melanie Budde, Piero Mazzolini, and Oliver Bierwagen

Efficient suboxide sources in oxide molecular beam epitaxy using mixed metal + oxide charges: The examples of SnO and Ga_2O

Cite as: APL Mater. 8, 031110 (2020); doi: 10.1063/1.5134444
Submitted: 30 October 2019 • Accepted: 21 February 2020 •
Published Online: 12 March 2020

Georg Hoffmann,[a] Melanie Budde,[b] Piero Mazzolini,[c] and Oliver Bierwagen[d]

AFFILIATIONS

Paul-Drude-Institut für Festkörperelektronik, Leibniz-Institut im Forschungsverbund Berlin e.V., Hausvogteiplatz 5-7, 10117 Berlin, Germany

[a]**Author to whom correspondence should be addressed:** hoffmann@pdi-berlin.de
[b]budde@pdi-berlin.de
[c]mazzolini@pdi-berlin.de
[d]bierwagen@pdi-berlin.de

ABSTRACT

Sources of suboxides, providing several advantages over metal sources for the molecular beam epitaxy (MBE) of oxides, are conventionally realized by decomposing the corresponding oxide charge at extreme temperatures. By quadrupole mass spectrometry of the direct flux from an effusion cell, we compare this conventional approach to the reaction of a mixed oxide + metal charge as a source for suboxides with the examples of $SnO_2 + Sn \rightarrow 2\ SnO$ and $Ga_2O_3 + 4\ Ga \rightarrow 3\ Ga_2O$. The high decomposition temperatures of the pure oxide charge were found to produce a high parasitic oxygen background. In contrast, the mixed charges reacted at significantly lower temperatures, providing high suboxide fluxes without additional parasitic oxygen. For the SnO source, we found a significant fraction of Sn_2O_2 in the flux from the mixed charge that was basically absent in the flux from the pure oxide charge. We demonstrate the plasma-assisted MBE growth of SnO_2 using the mixed Sn + SnO_2 charge to require less activated oxygen and a significantly lower source temperature than the corresponding growth from a pure Sn charge. Thus, the sublimation of mixed metal + oxide charges provides an efficient suboxide source for the growth of oxides by MBE. Thermodynamic calculations predict this advantage for further oxides as well, e.g., SiO_2, GeO_2, Al_2O_3, In_2O_3, La_2O_3, and Pr_2O_3.

I. INTRODUCTION

The desire of mankind for faster and smaller devices has driven Si-based semiconductor technology to be scaled to the verge of its physical limits. Metal oxides (MOs) are promising candidates to overcome these limitations since they not only can compete with Si-based devices but also allow for new device concepts due to the wide tunability of their physical properties.[1] Regarding the fabrication of MOs, molecular beam epitaxy (MBE) is a powerful tool for the growth of single crystalline thin films and their heterostructures.[2–4]

In MBE, semiconducting oxides (e.g., ZnO,[5] SnO_2,[6,7] In_2O_3,[7,8] and Ga_2O_3[7,9,10]) have typically been grown by the reaction of the vapor from a metal charge placed in a heated effusion cell with reactive oxygen (an oxygen plasma or ozone) on the heated substrate in an ultra-high vacuum chamber. This approach comes at the price of (i) a reduced lifetime of filaments in the growth chamber due to their gradual oxidation by the supplied reactive oxygen or the necessity to use expensive, (more) oxidation-resistant parts and (ii) an unintentional oxidation of the elemental source charge and related flux instabilities, observed, e.g., for Si-doping of Ga_2O_3 using a Si charge.[11]

A potential solution to both problems is the use of oxide source charges to provide metal-oxide molecules instead of metal atoms to the growth surface, thus requiring no or less additionally supplied oxygen, i.e., a lower background oxygen pressure. Early high-temperature vaporization studies of rare-earth oxides[12] and other metal oxides[13] have shown that the main metal-containing constituents of the vapor are suboxide molecules in

many cases, e.g., Ga_2O or SnO from the sublimation of Ga_2O_3 and SnO_2. (The presence of rare-earth suboxides in the source vapor[12] also explains why additionally supplied molecular oxygen is still needed during the growth of rare-earth oxides from sublimed oxide charges.)[14] Thus, dielectric rare-earth oxides (e.g., Pr_2O_3, Nd_2O_3, La_2O_3, Gd_2O_3, Lu_2O_3)[14,15] or Ga_2O_3 as dielectric for III–V devices[16,17] have been typically grown by the sublimation of an oxide charge. Recently, during MBE growth in the presence of additionally supplied reactive oxygen, the sublimation of an SnO_2 charge has been used for Sn-doping of Ga_2O_3[10] and has become state-of-the-art for growing the complex oxide $BaSnO_3$,[3,18,19] and the sublimation of a Ga_2O_3 charge has been demonstrated for the growth of semiconducting Ga_2O_3.[20] MBE growth of $BaSnO_3$,[19] SnO,[21] and Ga_2O_3[22] from the oxide charge has been demonstrated to proceed even in the absence of additionally supplied oxygen.

The suboxides Ga_2O, SnO, and In_2O have also been detected as volatile, desorbing species during plasma-assisted MBE growth of Ga_2O_3,[9,23] SnO_2,[6,7] and In_2O_3[24] from the metal vapor since they are formed as an intermediate product on the surface of the growing oxide films.[25] Thus, besides reducing the required additional oxygen supply, the use of suboxide sources provides simpler growth kinetics by circumventing suboxide formation on the growth surface[25] and it provides suboxide molecules as building blocks for the growth of complex oxides similar to the enabling role of the SnO_2 charge for the growth of high-quality $BaSnO_3$.[3]

This advantage, however, comes at the price of a significantly higher source temperature (e.g., 1700 °C for Gd_2O_3[14] often realized by electron–beam evaporation,[15] or ≈1800 °C for Ga_2O_3 requiring the use of an Ir-crucible[20]) compared to that of the corresponding metal charge (e.g., <1000 °C for Ga) required to provide the same (useful) growth rate. Detailed inspection of early high-temperature vaporization studies of oxides,[13] however, reveals that the decomposition of heated mixtures of Sn and SnO_2 or Ga and Ga_2O_3 requires significantly lower temperatures than that of SnO_2 or Ga_2O_3 to produce the same suboxide flux. This is in agreement with the observation that Sn, Ga, and In-vapor can rapidly etch SnO_2, Ga_2O_3, and In_2O_3 films in vacuum even at typical growth temperatures (~600 °C) by the reactions $SnO_2 + Sn \rightarrow 2\ SnO$, $4\ Ga + Ga_2O_3 \rightarrow 3\ Ga_2O$, and $4\ In + In_2O_3 \rightarrow 3\ In_2O$ followed by desorption of the formed, volatile suboxides.[7]

In this work, we compare the approach of subliming mixtures of metal and oxide to the conventional one of subliming the pure oxide aiming at efficient suboxide sources for oxide MBE with the examples of Sn/SnO_2 and Ga/Ga_2O_3. For this purpose, the temperature-dependent flux of different source charges was investigated by quadrupole mass spectrometry with respect to the contained species and their partial pressure. The experiments were conducted in both vacuum and an oxygen background typical for an oxide MBE growth chamber. The advantages and disadvantages of the investigated approaches will be discussed, concluding with the recommendation of using mixed metal + oxide charges for efficient suboxide sources and the demonstration of SnO_2 growth by plasma-assisted MBE from the mixed Sn + SnO_2 charge. We show that our experimental results largely agree with thermodynamic calculations, which allow us to predict further oxides that can benefit from using the mixed metal + oxide charges as a suboxide source.

II. THERMODYNAMIC PREDICTIONS

To predict the resulting gaseous species and their vapor pressure as a function of temperature for the decomposition of the mixed metal-oxide charges in comparison with that of the pure oxide and the pure metal charges, we calculated the phase diagrams as well as amount and type of reaction products in thermodynamic equilibrium using the FactSage 7.3 software package.[26] Figures 1(a) and 1(b) show the corresponding phase diagrams. For the mixed charges, the (thick black) lines between the phases "Sn(l) + SnO_2(s)" and "SnO_2(s) + ideal gas" as well as "Ga(l) + Ga_2O_3(s)" and "Ga_2O_3(s) + ideal gas" denote the formation of the gaseous suboxide "SnO" as well as "Ga_2O" from the mixed charges [generally, the "ideal gas" phase refers to gaseous species that are given in Figs. 1(c) and 1(d)]. These lines are, thus, indicating the vapor pressure of the suboxides as a function of source temperatures for the mixed charge. Note, the co-existing solid SnO_2 as well as Ga_2O_3 with the suboxide ideal gas phase is due to the oxide-rich stoichiometry of the source charge chosen in our experiments. At higher temperature, this remaining solid SnO_2 as well as Ga_2O_3 decomposes and sublimes at the boundary to the phase "ideal gas." This boundary is agreeing well with the decomposition and sublimation of the pure oxides, i.e., the boundary between the phases "SnO_2(s)" and "Ga_2O_3(s)" and "ideal gas" marked by a thick red line.

The comparison of the (thick black) boundaries between the mixed metal-oxide phases and oxide + ideal gas to the (thick red) boundaries between the solid oxides and ideal gas clearly predicts the potential advantage of a lower source temperature required to achieve a certain suboxide vapor pressure when the metal-oxide mixtures are used. In addition, this charge requires even lower source temperatures than the metal charge to achieve the same predicted vapor pressure as comparison to the (thick green) boundary between the liquid and gaseous metals. In our MBE system, a growth rate on the order of 1 Å/s relates to a partial pressure of the source material in the effusion cell on the order of 10^{-3} mbar. Figure 1(a) suggests that this partial pressure requires source temperatures of ≈760 °C, ≈1050 °C, and ≈1090 °C for the mixed SnO_2 + Sn, pure SnO_2, and pure Sn charge, respectively. In comparison, the mixed Ga_2O_3 + Ga, pure Ga_2O_3, and pure Ga charge source temperatures of ≈630 °C, ≈1320 °C, and ≈920 °C, respectively, would be required.

Figures 1(c) and 1(d) shows the composition of the equilibrium reaction products, particularly that of the "ideal gas," from the mixed metal-oxide source charges as a function of temperature T at a fixed total pressure of $P = 10^{-3}$ mbar. The formation of an ideal gas phase that exclusively consists of $(SnO)_x$ and Ga_2O can be seen when T exceeds ≈760 °C and ≈630 °C for the SnO_2 + Sn and Ga_2O_3 + Ga charge, respectively. The remaining solid SnO_2 and Ga_2O_3 decompose at about 1050 and 1250 °C, respectively, by the formation of suboxide and oxygen species. Importantly, at ≈1500 °C and ≈1250 °C, additional gaseous Sn and Ga, respectively, as well as oxygen species are formed coinciding with a reduced formation of suboxide molecules. These results predict pure suboxide fluxes from the mixed charges, an additional oxygen fraction in the fluxes from the pure oxide charges, and another additional Ga fraction in the flux from pure Ga_2O_3 charges.

Figures S1–S6 in the supplementary material show phase diagrams for further mixed metal + oxide charges, i.e., Al_2O_3 + Al,

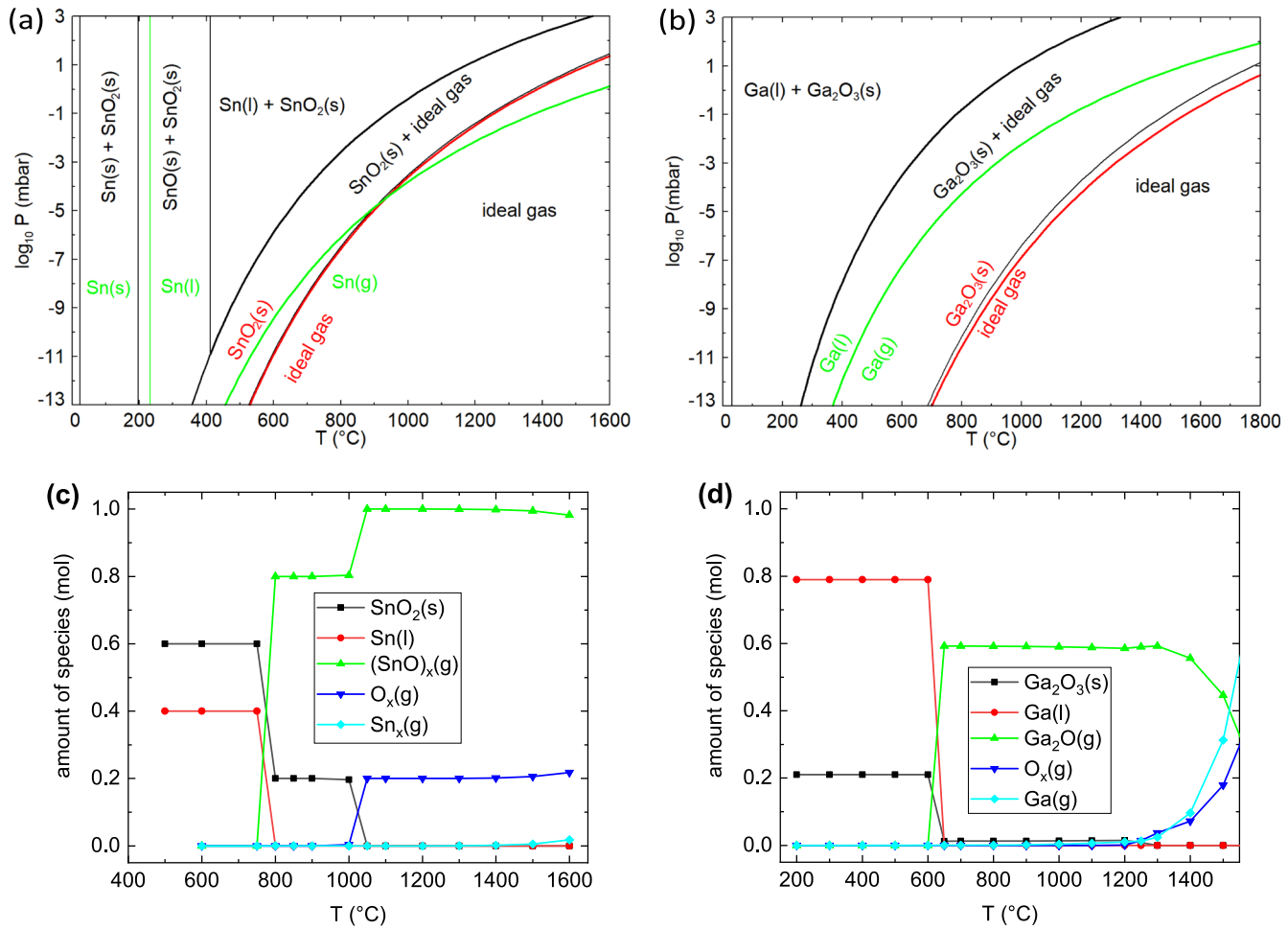

FIG. 1. (a) and (b) Phase diagrams comparing charges of pure oxide (red), mixed metal-oxide (black), and pure metal (green). Phases denoted "s" are solid, those denoted "l" are liquid. Gas phases are denoted "g" or "ideal gas" in case of gas mixture. The compositions of the "ideal gas" phase of the mixed charges are given in (c, d). (c) and (d) Molar fraction of equilibrium reaction products of the used mixed charges as a function of temperature at a fixed total pressure of $P = 10^{-3}$ mbar that corresponds to a typical pressure inside the effusion cell during oxide MBE. (a) and (c) The case of pure SnO_2 compared to 0.6 mol SnO_2 + 0.4 mol Sn and pure Sn. (b) and (d) The case of pure Ga_2O_3 compared to 0.21 mol Ga_2O_3 + 0.79 mol Ga and pure Ga.

In_2O_3 + In, SiO_2 + Si, GeO_2 + Ge, La_2O_3 + La, and Pr_2O_3 + Pr, that are predicted to result in suboxide vapors. Similar thermodynamic calculations for Nd_2O_3 + Nd, Gd_2O_3 + Gd, and Lu_2O_3 + Lu resulted in metal vapor instead of suboxide vapor.

III. EXPERIMENTAL

For the present study, a high temperature single filament effusion cell (CreaTec) with a 10 cm^3 Al_2O_3 crucible was mounted opposite to a quadrupole mass spectrometer (QMS; model HALO 201 HidenAnalytical) in a custom-built, tube-shaped vacuum chamber with an approximate volume of 5500 cm^3. The electron energy of the ionizer inside the QMS can be tuned in a range from 6 eV to 120 eV. In this setup, schematically shown in the inset of Fig. 2(a), the front end of the effusion cell directly points at that of the QMS with a distance of ~60 cm in between. A shutter between the effusion cell and QMS allowed interrupting the flux to the QMS. The system is connected to a turbo molecular pump (with a pumping capacity for N_2 of 400 l/s) that maintained a background pressure in the range of 10^{-8} to 10^{-7} mbar measured by an ion gauge. To simulate the background pressures in an oxide-MBE system, a variable leak valve allowed molecular oxygen (99.99% purity) to be provided to the system. For the SnO suboxide study, the following charges were investigated: SnO_2 powder (4N), SnO powder (3N), Sn slugs (5N), and a mixture of 60 mol. % SnO_2 and 40 mol. % Sn. For the Ga_2O suboxide study, the studied charges were Ga_2O_3 powder (5N), Ga slugs (7N), and a mixture of 21 mol. % Ga_2O_3 and 79 mol. % Ga. The molar percentages were chosen in such a way that only oxide will remain in the cell when the charge is used up completely for suboxide formation. After inserting the effusion cell, the vacuum chamber was evacuated and the cell was outgassed. The source materials were heated up to typical sublimation temperatures, and mass spectra of the emitted species were recorded at different cell temperatures

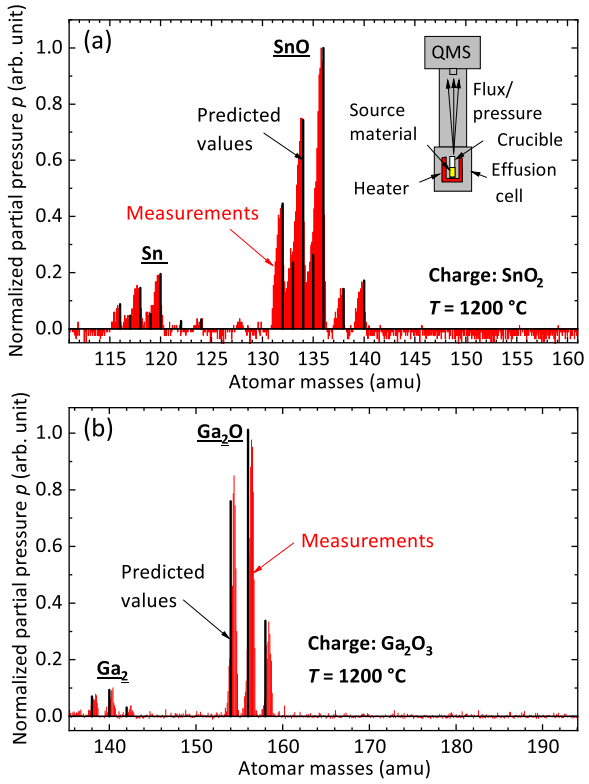

FIG. 2. (a) QMS spectrum of Sn and SnO (red lines) measured at 1200 °C using a SnO_2 charge. Inset: Sketch of the system. (b) QMS spectrum of Ga_2O and Ga_2 from a Ga_2O_3 charge at 1200 °C. Due to the isotopic distribution (black lines), the species can be easily identified.

and background oxygen pressures as follows and also described in Sec. IV.

For the Sn-related system, we monitored only isotopes with the highest natural abundance, i.e., Sn and SnO, at 120 amu and 136 amu with an abundance of 32.6% and Sn_2, Sn_2O, and Sn_2O_2 at 238 amu, 254 amu, and 270 amu with an abundance of 17.1%, respectively. Note that for molecules containing two Sn atoms, the probabilities of all isotopic combinations which, i.e., result in 270 amu have been summed up. For Ga, we observed a parasitic background signal at 69 amu. As a consequence, we monitored the peak related to ^{71}Ga, with a natural abundance of 39.9% for Ga, whereas for GaO, the isotope at 85 amu with an abundance of 60.1% was tracked. For Ga_2 and Ga_2O, we monitored the isotopes with the highest abundance of 48% at 140 amu and 156 amu, respectively. The QMS is calibrated for N_2 regarding ionization cross section σ and multiplier efficiency γ measuring the investigated species in terms of partial pressure. In our measurements, no correction was made to account for the different sensitivity of the QMS to the investigated species. As a consequence of this and the fact that we did not measure all isotopes, the partial pressures in our discussion are given in arbitrary units (arb. unit). Nevertheless, partial pressures of the same species can be quantitatively compared among different charges since they all were measured in the same manner. In order to relate the measured fluxes to actual growth rates for the Sn-related system, we conducted deposition experiments on Si substrates mounted at a distance of ≈30 cm away from the source. A discussion of the deposition rates will be given in Secs. IV C and IV D.

Finally, as an initial application test of our mixed SnO source scheme, we mounted a dual filament effusion cell with a mixed Sn + SnO_2 charge inside a pyrolytic boron nitride (BN) crucible in a plasma-assisted MBE growth chamber. The BN crucible allowed us to run the hot lip of the cell 150 K hotter than the base to prevent clogging of the source. (Care has to be taken when venting or pumping the growth chamber to prevent the oxide powder from being blown out of the cell.) For comparison to the growth of SnO_2 from the pure metallic Sn charge, a single filament effusion cell filled with Sn was also mounted on the growth chamber. Activated oxygen was supplied by a defined flow of molecular oxygen passed through an RF plasma source run at a constant RF power of 300 W. Laser reflectometry (LR) allowed us to measure the growth rate *in situ* during growth as described in Ref. 7.

A great advantage of the QMS is its sensitivity to the smallest amounts of emitted species from the source charge as well as the ability to distinguish different isotopes, leading to unique fingerprints. In Figs. 2(a) and 2(b), typical QMS spectra are shown. Due to the isotopic distribution of Sn,[27] the Sn and SnO signals in Fig. 2(a) can be clearly identified (black solid lines). Note that no SnO_2 was recorded. In Fig. 2(b), the recorded QMS spectra show the presence of Ga_2O and Ga_2, whereas no Ga_2O_3 was recorded. Also here, the isotopic distribution[27] allows for a clear identification of the molecules sublimed from the source material Ga_2O_3.

A frequently observed problem in QMS, however, is cracking of molecules from the direct flux inside the ionizer of the QMS. The resulting cracking products show up as additional species in the mass spectra. Cracking products can be distinguished from parent molecules of the direct flux by determining the minimum electron energy required for their ionization (and thus detection), the so called *appearance potentials*. The appearance potential of a cracking product A from a species AX should be higher than that of the same species A in the direct flux, as additional energy to that of ionization of A is required for cracking the parent species AX.[28] An example of this behavior is shown in Fig. 3. The Sn

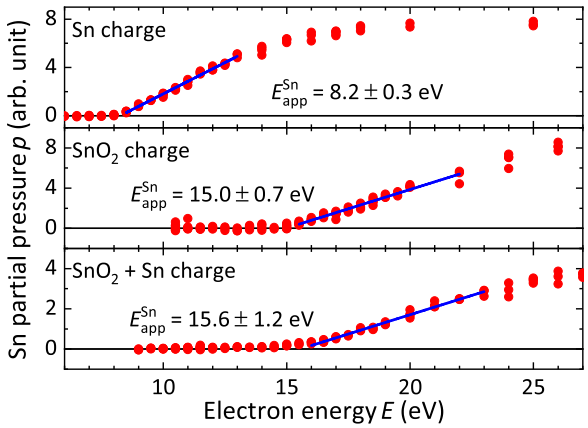

FIG. 3. QMS signals of Sn from the three different charges Sn, SnO_2, and SnO_2 + Sn as a function of electron ionization energy. From the linear fit (blue solid line), the appearance potentials were determined.

signal from a Sn charge which we used as a reference for the Sn signal (upper graph) rises from the background at significantly lower electron energy compared to the ones from the SnO_2 and SnO_2 + Sn charges (middle and lower graph). Considering the SnO dissociation energy of 5.44 eV[29] which is similar to the difference of the Sn appearance potentials in Fig. 3, we assume the Sn signal from the SnO_2 and SnO_2 + Sn charges to be a fragment which is created in the QMS by cracking and ionization processes.

IV. RESULTS AND DISCUSSION

A. Species in the SnO source flux

For all charges, QMS spectra at sufficiently high temperatures were recorded. The detected species of the different charges and their appearance potentials are listed in Table I. In addition, we marked the parent ions and the fragments by p and f, respectively, as discussed above.

The SnO_2 + Sn mixture and the SnO charge resulted in the same appearance potentials within their uncertainty. Assuming that SnO decomposes into 50 mol. % SnO_2 and 50 mol. % Sn above 400 °C, no difference in the behavior of the SnO_2 + Sn charge and the SnO charge in terms of the constituents coming out from the cell can be made. In the following, only the mixture will be discussed since the purity of the components for SnO_2 + Sn charge is higher compared to that of SnO, and therefore, is more suitable for oxide MBE. All results are shown in Table I. A comparison of our results to those from other groups in the same table shows a good agreement. As discussed for Fig. 3 and following the argumentation in the literature,[27,29,30] we identified SnO and Sn_2O_2 to be parent ions for the SnO_2 charge and Sn to be a fragment created in the QMS. For the SnO_2 + Sn charge, SnO and Sn_2O_2 were determined to be parent ions, while Sn, Sn_2, and Sn_2O were identified as fragments. Here, the energy gap between the Sn_2O_2 and the Sn_2O, as well as the gap between Sn_2O and Sn_2, and the gap between SnO and Sn are in good agreement with the binding energy of the SnO molecule (i.e., 5.44 eV).[29] The presence of Sn_2 ions at high electron energies indicates the potential existence of Sn_2O_2 molecules with Sn–Sn bonds.

From these results, we can confirm the following reactions within the different source charges:[29,30]

$$SnO_2(s) \Rightarrow \frac{1}{n}(SnO)_n(g) + \frac{1}{2}O_2(g), \quad (1)$$

$$\frac{1}{2}SnO_2(s) + \frac{1}{2}Sn(l) \Rightarrow \frac{1}{n}(SnO)_n(g), \quad (2)$$

$$\text{with } (n = 1, 2).$$

For Eq. (2) also, $n = 4$ and 6 have been measured by Zimmermann *et al.*[30]

B. Species in the Ga_2O source flux

For the Ga_2O suboxide sources, we performed the experiments in the same manner as for the SnO suboxide sources and summarize the detected species and appearance potentials for the different charges in Table II. The parent ions and fragments are, again, labeled with p and f, respectively.

From our results and in accordance with the literature,[31–33] we consider Ga_2O to be a parent ion for all investigated charges since we did not detect any Ga_2O_3 as potential parent ion of Ga_2O [see Fig. 2(b)]. We also assume Ga_2 to be a fragment for all investigated charges due to its high appearance potential that lies ~7 eV above the one of Balducci *et al.*, who investigated vapors of gallium–indium alloys.[33] Our data further indicates that the Ga and GaO signals recorded from the Ga_2O_3 + Ga mixture are fragments since their appearance potentials lie more than 5 eV above the findings of Burns, who also investigated solid and molten powder of Ga_2O_3 by electron bombardment (which, in contrast to our findings, also produces GaO parent ions).[31] In addition to that, the Ga_2O molecule is considered to have the symmetric structure Ga–O–Ga[34,35] and a GaO bond energy in the range of 5.3–5.4 eV,[32,36] from which we can draw the conclusion of Ga and GaO being created by fragmentation and ionization processes by simply adding up the energy contributions (as we did in the discussion about the SnO charges). We further assume the Ga and GaO signals of the Ga_2O_3 charge to be parent ions since their appearance potentials are very close to the values of Burns[31] and 4–5 eV below the ones we found for the Ga_2O_3 + Ga charge. The appearance potentials of the recorded Ga signal confirm

TABLE I. Appearance potentials of the different species from SnO_2 + Sn, SnO, SnO_2, and Sn charges as well as comparison to values derived from Zimmermann *et al.*[30] ("Zimm"), Colin *et al.*[29] ("Colin"), and Radzig and Smirnov[27] ("Radzig"). The parent ions as well as the fragments are labeled by p and f, respectively.

	Our measurements						
Charge	Sn	SnO_2	SnO_2 + Sn	SnO	Radzig	Colin	Zimm.
T_{Cell}	1050 °C	1200 °C	800 °C	800 °C	Sn	SnO_2/Sn + SnO_2	SnO_2 + Sn
Species	Appearance potentials (eV)						
Sn	8.7 ± 0.2 (p)	15.0 ± 0.7 (f)	15.6 ± 1.2 (f)	16.1 ± 0.5 (f)	7.3 ± 0.2 (p)	13.0 ± 1.0 (f)	13.5 ± 1.0 (f)
SnO		11.5 ± 0.4 (p)	11.1 ± 0.3 (p)	10.8 ± 0.7 (p)		10.5 ± 0.5 (p)	10.7 ± 0.5 (p)
Sn_2			20.3 ± 2.2 (f)	18.9 ± 2.4 (f)			
Sn_2O			14.5 ± 1.3 (f)	15.1 ± 1.1 (f)		13.8 ± 0.5 (f)	
Sn_2O_2		10.5 ± 0.8 (p)	9.9 ± 0.4 (p)	9.9 ± 0.4 (p)		9.8 ± 0.5 (p)	9.7 ± 0.5 (p)

TABLE II. Appearance potentials of the different species from Ga_2O_3 + Ga, Ga_2O_3, and Ga charges. For comparison, values derived from Burns[31,32] ("Burns") and Balducci *et al.*[33] ("Bald.") are shown.

	Our measurements			Burns	Bald.
Charge	Ga	Ga_2O_3 + Ga	Ga_2O_3	Ga_2O_3	Ga + In
Species	Appearance potentials (eV)				
Ga	6.6 ± 0.3 (p)	11.9 ± 0.4 (f)	7.5 ± 0.6 (p)	6.0 ± 0.3 (p)	6.0 ± 0.5 (p)
GaO		15.1 ± 1.8 (f)	11.4 ± 1.1 (p)	9.4 ± 0.5 (p)	
Ga_2		16.3 ± 1.4 (f)	14.9 ± 1.8 (f)		6.2 ± 0.5 (p)
Ga_2O		9.8 ± 0.5 (p)	9.7 ± 1.0 (p)	8.4 ± 0.6 (p)	

Ga to be a parent ion from the Ga charge in accordance with the values in the literature.[31,33]

Our results indicate the Ga_2O_3 charge to produce also Ga and GaO next to Ga_2O, while the Ga_2O_3 + Ga mixture produces a pure Ga_2O flux:

$$Ga_2O_3(s) \Rightarrow \frac{1}{2}\,Ga_2O(g) + \frac{1}{2}\,GaO(g) + \frac{1}{2}\,Ga(g) + O_2(g), \quad (3)$$

$$Ga_2O_3(s) + 4\,Ga(l) \Rightarrow 3\,Ga_2O(g). \quad (4)$$

Our findings are also in line with the results of Frosch and Thurmond[37] who also investigated the Ga_2O_3 + Ga mixture using a tube oven with the result that Ga_2O suboxide is formed according to Eq. (4).

C. Quantitative flux and activation energies of the SnO source

For the temperature dependent measurements, electron energies of 50 eV were used for the detection of the species to maximize the sensitivity. As a result, some of the measured signals might be affected by fragmentation.

After the identification of all parent ions of the SnO and Ga_2O suboxide sources, we measured the fluxes in terms of partial pressures at different temperatures. The recorded SnO partial pressures of the SnO_2 and SnO_2 + Sn charges are shown as Arrhenius plots in Fig. 4 along with the related activation energies. The activation energies of SnO and Sn_2O_2 from the SnO_2 charge are higher compared to the ones from the SnO_2 + Sn mixture. We observe a small deviation of the SnO flux from the ideal behavior to smaller partial pressures at higher temperatures for the measurements whose origin is unclear at present.

We extrapolated the estimated partial pressures at higher temperatures from the SnO activation energy (shown as red dotted line for the SnO_2 charge). In addition to the SnO suboxide, however, a non-negligible amount of the higher oligomer Sn_2O_2 is detected in the particle flux from the SnO_2 + Sn in contrast to the pure SnO_2 charge where the amount of Sn_2O_2 is about two orders of magnitude lower at the same SnO flux assuming similar detection probabilities of the species.[29] Further oligomers of Sn_xO_x with x = 4, 6, outside the mass-range of our QMS, were reported in the literature arising from the heated SnO_2 + Sn mixture.[29,30] Whether or not these oligomers are detrimental for the growth of SnO related oxides will be discussed later. According to Zimmermann *et al.*,[30] the partial pressure of SnO is only 13% of the total flux when using a mixture. In contrast to that, when using a SnO_2 charge, almost 100% of the total flux is given by the SnO. As a consequence of these findings, we added a green dotted line to Fig. 4 in which we multiplied the SnO signal of the mixture by a factor of 7.7 to account for all oligomers which contribute to the SnO deposition. Note that also here for higher temperatures, the values were extrapolated from the activation energy in the same way as for the red dotted line. We carried out deposition experiments to correlate the partial pressures to growth rates when using MBE. Therefore, Si wafers were mounted line of sight with the effusion cell at a distance of ≈30 cm away from the cell. A HF dip was carried out on the wafers to build a smooth surface. The deposition experiments lasted 4–6 h. The thickness of the films was determined by a profilometer and cross sectional SEM.

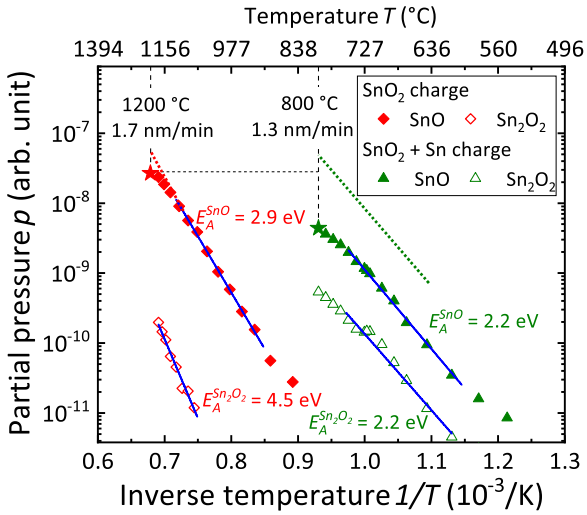

FIG. 4. Arrhenius diagram of the parent ion partial pressures for different SnO source charges listed in the legend. The blue lines denote the linear fit from which the activation energies were calculated. The detection limit is in the range of 10^{-12} arb. units. The red and green stars denote the partial pressure during the deposition experiments at 1200 °C and 800 °C for the SnO_2 charge and the SnO_2 + Sn charge, respectively. The corresponding deposition rates are written below the deposition temperature. The red dotted line marks the extrapolation of the total amount of SnO to 1200 °C for the SnO_2 charge. The green dotted line marks an upper limit for the partial pressure taking all SnO oligomers into account which contribute to the SnO deposition using the SnO_2 + Sn charge.

Source temperature and deposition rates are also added to Fig. 4, and the corresponding partial pressures are marked as stars. We assume the partial pressure of the sum of all $(SnO)_x$, x = 1, 2, 4, 6 oligomers to be in the region between the green dotted line and the green triangles according to the value of the deposition rate. The measurements reveal the advantage of the SnO_2 + Sn mixture since the same SnO flux can be reached at cell temperatures ≈400 K below the ones needed for the SnO_2 charge, exemplified by the black dashed lines and corresponding deposition rates in Fig. 4. Given the experimental uncertainties, this temperature difference is in fair agreement with the theoretically predicted one of ≈300 K [cf. Fig. 1(a)]. Growth rates in our MBE chamber from the mixed charge will be discussed in Sec. IV F. For growth rates of $BaSnO_3$ on the order of 0.2 Å/s, the authors of Refs. 18 and 19 have used an SnO_2 cell temperature of ≈1100 °C[38,39] corresponding to an SnO flux of 8×10^{13} cm^{-2} s^{-1}.[38] According to our theoretical predictions and experimental results in Figs. 1(a) and 4, the same flux can be obtained from mixed Sn + SnO_2 charge at a 300–400 K lower cell temperature.

During sublimation from the SnO_2 + Sn charge as well as from the SnO charge, solid SnO accumulates at the top of the single-filament cell closing the cell aperture completely. Figure S7 in the supplementary material shows the partially closed cell after sublimation of a quantity of SnO at 850 °C for 1 h. This detrimental effect can be avoided by the use of a hot-lip cell with a PBN crucible and a temperature difference of 150 °C between the crucible and the lip.

D. Quantitative flux and activation energies of the Ga_2O source

For the Ga_2O suboxide sources, we proceeded in the same manner as for the SnO suboxide sources. In Fig. 5, the fluxes of the Ga_2O suboxide from Ga_2O_3, and Ga_2O_3 + Ga charges are shown. The authors of Ref. 20 grew 160 nm-thick Ga_2O_3 layers by MBE from a Ga_2O_3 charge heated to ≈1800 °C. Assuming a typical growth time on the order of 1 h, this would correspond to a growth rate on the order of ≈0.5 Å/s. As shown in Fig. 5, the same growth rate could be achieved by using the Ga_2O_3 + Ga charge at temperatures that are ≈700 °C lower than the ones needed for the bare Ga_2O_3 charge. [Comparison to the theoretically predicted Ga_2O vapor pressures in Fig. 1(b), however, suggests 1800 °C or 1100 °C to be significantly too high for typical MBE growth rates.] This is likely related to the significantly lower activation energy for the Ga_2O formation from the reaction of Ga with Ga_2O_3 compared to that for the decomposition of pure Ga_2O_3. Moreover, the Ga_2O flux from the Ga_2O_3 + Ga charge does not contain measurable additional Ga in contrast to that from the pure Ga_2O_3 charge (see discussion of appearance potentials). Due to these findings, the use of the Ga_2O_3 + Ga mixture as Ga_2O suboxide source seems to be a promising candidate for both highly pure Ga_2O suboxide fluxes at adequate cell temperatures using standard cell crucibles and longer lifetimes of inner MBE components.

E. Role of oxygen background

Next, we investigated the quantitative influence of an externally supplied oxygen background on the sublimation of the suboxides from the different charges. This situation mimics typical growth

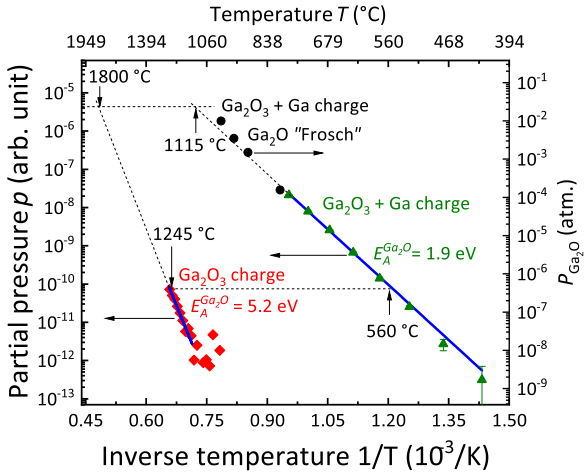

FIG. 5. Arrhenius diagram of the parent ion partial pressures for different Ga_2O source materials (left axis). The blue lines denote the fit from which the activation energies E_A for the Ga_2O signals were calculated. The detection limit is in the range of 10^{-12} arb. units. The signals were extrapolated to higher temperatures for comparison with other groups. The black circles (right axis) are Ga_2O suboxide pressures from Frosch and Thurmond ("Frosch")[37] using a mixture of Ga + Ga_2O_3. The data were added to the graph with respect to the right axes. The temperatures of the Ga_2O_3 charge and the mixed Ga_2O_3 + Ga charge required to reach the same suboxide flux (marked by the horizontal dotted lines) are indicated by vertical arrows.

conditions in an oxide MBE growth chamber as some form of oxygen is typically required to oxidize the metal or suboxide vapors toward the "full" oxide on the substrate surface. When the mixtures SnO_2 + Sn or Ga_2O_3 + Ga are used, no changes of the suboxide flux according to Eqs. (2) and (4) were observed. The same conclusions could be made for the SnO_2 and Ga_2O_3 charges. However, at high oxygen background pressures $p_{O_2} = 10^{-6}$–10^{-5} mbar, we observed a slight decrease in the suboxide signals by 10%–30% (see Fig. S8 in the supplementary material) which could be important for cell flux calibration in oxide MBE. The origin of this decrease could be attributed to a reduced mean free of the molecules in the chamber or might be related to a reduced vapor pressure which is caused by the high amount of oxygen.

Furthermore, sublimation of the pure oxide charges coincides with its decomposition.[14,20] The consequential oxygen loss can have a non-negligible contribution to the oxygen background pressure in the growth chamber. (Indeed, this parasitic oxygen background has even been used for growth of Ga_2O_3 from the pure oxide charge.[20]) Figure 6 shows the oxygen background pressure measured with the QMS during sublimation of the pure oxide charges in comparison to that of the mixed charge in our setup, both in the absence of additionally supplied oxygen. A clear increase in the oxygen partial pressure with temperature of the SnO_2 and Ga_2O_3 charges is observed according to the reaction given in Eqs. (1) and (3), respectively. The trends evidence the creation of a significant oxygen background at cell temperatures required for typical growth rates (e.g., 1100 °C for SnO_2 and >1300 °C for Ga_2O_3 charges) with the pure oxide charge. This parasitic oxygen background prevents access to oxygen poor growth conditions. In contrast, the significantly lower cell

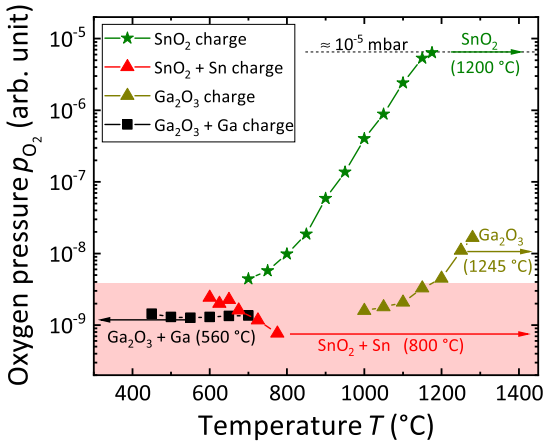

FIG. 6. Comparison of the oxygen background created during sublimation of the pure oxide charges and sublimation of the mixed (oxide + metal) charges: Oxygen background pressure p_{O_2} dependence on the temperature T of the SnO_2, SnO_2 + Sn, Ga_2O_3, and Ga_2O_3 + Ga charges. The arrows mark the oxygen background pressures created from SnO_2 vs SnO_2 + Sn and Ga_2O_3 vs Ga_2O_3 + Ga charges at the given temperatures that lead to the same suboxide flux (given as horizontal dotted lines in Figs. 4 and 5, respectively). The dotted line denotes the background pressure of 10^{-5} mbar measured by an ion gauge for the SnO_2 charge at 1200 °C. The red shaded area denotes the typical oxygen background pressure in the evacuated system.

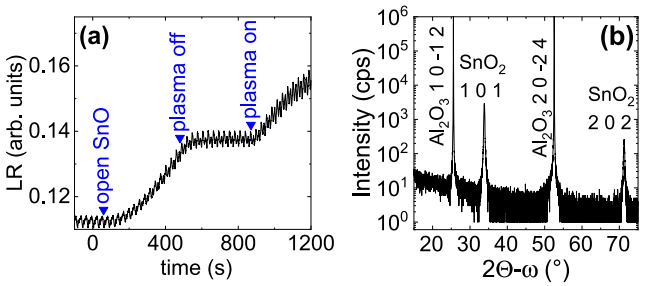

FIG. 7. Plasma-assisted MBE growth of SnO_2 on r-plane sapphire using the Sn + SnO_2 mixed charge. (a) Laser reflectometry signal during the beginning of growth demonstrating no growth without plasma activation. The high-frequency oscillations are an artifact of the substrate rotation. (b) XRD symmetric out-of-plane $2\Theta - \omega$ scan of the resulting layer demonstrating single-phase, epitaxial SnO_2. The diffraction peaks are labeled.

temperatures required for the same growth rate (or suboxide flux) from the mixed oxide + metal charges prevents the oxide decomposition with oxygen release, supporting the assumption of the reactions given by Eqs. (2) and (4) taking place directly in the crucible. Thus, the use of the mixed charges prevents the formation of a significant parasitic oxygen background as exemplified by the arrows in Fig. 6.

F. Plasma-assisted MBE growth of SnO_2 using the mixed Sn + SnO_2 charge

As application example, an SnO_2 film was grown from the mixed SnO source at a substrate temperature of 800 °C, a SnO base temperature of 810 °C (hot lip at 960 °C), and an oxygen flow of 0.5 standard cubic centimeters per minute (sccm). (Note that these growth conditions have not been optimized.) We used an r-plane sapphire substrate that has been shown to lead to the formation of (101)-oriented, single crystalline films by plasma-assisted MBE growth from the metallic source.[40,41] Figure 7(a) shows the LR trace of the initial growth phase in our experiment where the oxygen flow and plasma had been turned on before time $t = 0$ s. The increasing LR signal after opening the SnO shutter indicates film growth. At $t = 480$ s, the plasma was turned off, maintaining the molecular oxygen flow. The plateau in the LR signal indicates that growth ceased at this point, demonstrating the need of activated oxygen to oxidize SnO in our MBE environment. Growth continued when the plasma power was turned back on at $t = 870$ s as indicated by the further increasing LR signal. Figure 7(b) shows the out-of-plane symmetric $2\Theta - \omega$ x-ray diffraction (XRD) scan of the ≈300 nm-thick (estimated from oscillations in the LR signal) final layer after a total growth time of ≈100 min, confirming growth of an epitaxial SnO_2(101) layer using the SnO source and plasma-activated oxygen.

For comparison to growth of SnO_2 using an Sn source, we operated the SnO and the Sn source at similar fluxes that correspond to growth rates of 0.95 and 1.2 Å/s, respectively, under conditions of full cation incorporation into the SnO_2 film. The corresponding cell temperatures of the Sn and the SnO sources were 1175 °C and 815 °C (hot lip 965 °C), respectively, being in good agreement with the thermodynamic predictions in Fig. 1(a). At a substrate temperature of 700 °C, the growth rate as a function of activated oxygen flow was determined by LR for the growth on c-plane Al_2O_3 substrates for both sources individually. An oxygen flow of 0.15 sccm enabled a growth rate of 0.99 Å/s for growth from the SnO source. At the same oxygen flow, the growth rate using the Sn source was as low as 0.2 Å/s and an oxygen flow of 0.32 sccm was required to achieve a growth rate of 0.9 Å/s (i.e., almost full Sn incorporation into the film). Our results confirm two advantages of the SnO source using a mixed Sn + SnO_2 charge over an Sn source: (1) Less (but activated) oxygen is required for the growth of SnO_2, and (2) a significantly lower cell temperature is required to obtain the same growth rate.

V. SUMMARY AND CONCLUSION

In summary, an effusion cell with SnO_2 or Ga_2O_3 charge and mixed Sn + SnO_2 or Ga + Ga_2O_3 charge was investigated as a source of the suboxide SnO or Ga_2O, respectively, for the oxide growth by MBE. For this purpose, the direct flux from the cell run at temperatures up to 1280 °C was analyzed by quadrupole mass spectrometry in vacuum without and with an externally supplied oxygen background pressure up to 10^{-5} mbar, the latter one mimicking typical conditions in an oxide MBE growth chamber. These source scenarios were also assessed by thermodynamic calculations that predict the vapor pressure of the resulting species as well as approximate source temperatures for typical MBE growth rates.

The high temperature required for a realistic suboxide flux from the conventionally used oxide charge (SnO_2 or Ga_2O_3) results in an appreciable background of oxygen created by the decomposition of the source material. In addition, metallic Ga was detected in the vapor from the Ga_2O_3 charge.

An efficient alternative is the mixed metal + oxide charge, producing a metal-free suboxide flux at lower activation energy and significantly lower cell temperature without measurable creation and emission of additional oxygen. These lower cell temperatures allow the use of standard effusion cells and crucibles (e.g., PBN, Al_2O_3) but require the use of a hot-lip effusion cell in the case of SnO to prevent clogging of the cell by solid SnO deposits at the tip of the crucible. The mixed SnO_2 + Sn charge creates a significant fraction of higher oligomers (e.g., Sn_2O_2), which is almost absent in the case of the pure SnO_2 charge. We further demonstrated that plasma-assisted MBE of an epitaxial SnO_2 film from the mixed SnO source allows for a lower activated oxygen flux and cell temperature than the corresponding growth from an Sn source.

We conclude that mixed metal + oxide charges are a promising, efficient source of suboxides that can outrival the pure oxide charge. Our results are generally applicable to further oxides (e.g., In_2O_3, Al_2O_3, La_2O_3, Pr_2O_3, GeO_2, SiO_2) that possess suboxides (e.g., In_2O, Al_2O, LaO, PrO, GeO, SiO), as well as selenides, sulfides, and tellurides that possess respective subcompounds (e.g., Ga_2Se, In_2Se, SnSe, In_2S, In_2Te).

SUPPLEMENTARY MATERIAL

The supplementary material contains phase diagrams similar to Figs. 1(a) and 1(b) of the metal + oxide charges: Al_2O_3 + Al, In_2O_3 + In, SiO_2 + Si, GeO_2 + Ge, La_2O_3 + La, and Pr_2O_3 + Pr. It further contains a photograph of the clogged SnO cell and the measured suboxide flux from the mixed charges SnO_2 + Sn and Ga_2O_3 + Ga as a function of externally supplied oxygen.

ACKNOWLEDGMENTS

The authors thank Steffen Behnke for the technical support and construction work on the system, Christian Roethlein for his support on the QMS system, Zbigniew Galazka for providing SnO_2 and Ga_2O_3 powders, and Stefano Cecchi for the critical reading of the manuscript. This work was performed in the framework of GraFOx, a Leibniz-ScienceCampus partially funded by the Leibniz association. Financial support of this work by the Leibniz association under Grant No. K74/2017 is gratefully acknowledged.

REFERENCES

[1] X. Yu, T. J. Marks, and A. Facchetti, "Metal oxides for optoelectronic applications," Nat. Mater. **15**(4), 383–396 (2016).
[2] D. G. Schlom, "Perspective: Oxide molecular-beam epitaxy rocks!," APL Mater. **3**(6), 062403 (2015).
[3] S. Raghavan, T. Schumann, H. Kim, J. Y. Zhang, T. A. Cain, and S. Stemmer, "High-mobility $BaSnO_3$ grown by oxide molecular beam epitaxy," APL Mater. **4**(1), 016106 (2016).
[4] M. Higashiwaki, K. Sasaki, A. Kuramata, T. Masui, and S. Yamakoshi, "Gallium oxide (Ga_2O_3) metal-semiconductor field-effect transistors on single-crystal β-Ga_2O_3 (010) substrates," Appl. Phys. Lett. **100**(1), 013504 (2012).
[5] Y. Nishimoto, K. Nakahara, D. Takamizu, A. Sasaki, K. Tamura, S. Akasaka, H. Yuji, T. Fujii, T. Tanabe, H. Takasu, A. Tsukazaki, A. Ohtomo, T. Onuma, S. F. Chichibu, and M. Kawasaki, "Plasma-assisted molecular beam epitaxy of high optical quality MgZnO films on Zn-polar ZnO substrates," Appl. Phys. Express **1**(9), 091202 (2008).
[6] M. Y. Tsai, M. E. White, and J. S. Speck, "Investigation of (110) SnO_2 growth mechanisms on TiO_2 substrates by plasma-assisted molecular beam epitaxy," J. Appl. Phys. **106**(2), 024911 (2009).
[7] P. Vogt and O. Bierwagen, "The competing oxide and sub-oxide formation in metal-oxide molecular beam epitaxy," Appl. Phys. Lett. **106**(8), 081910 (2015).
[8] A. Bourlange, D. J. Payne, R. G. Egdell, J. S. Foord, P. P. Edwards, M. O. Jones, A. Schertel, P. J. Dobson, and J. L. Hutchison, "Growth of In_2O_3(100) on Y-stabilized ZrO_2(100) by O-plasma assisted molecular beam epitaxy," Appl. Phys. Lett. **92**(9), 092117 (2008).
[9] M. Y. Tsai, O. Bierwagen, M. E. White, and J. S. Speck, "β-Ga_2O_3 growth by plasma-assisted molecular beam epitaxy," J. Vac. Sci. Technol., A **28**(2), 354–359 (2010).
[10] K. Sasaki, A. Kuramata, T. Masui, E. G. Víllora, K. Shimamura, and S. Yamakoshi, "Device-quality β-Ga_2O_3 epitaxial films fabricated by ozone molecular beam epitaxy," Appl. Phys. Express **5**(3), 035502 (2012).
[11] N. K. Kalarickal, Z. Xia, J. McGlone, S. Krishnamoorthy, W. Moore, M. Brenner, A. R. Arehart, S. A. Ringel, and S. Rajan, "Mechanism of Si doping in plasma assisted MBE growth of β-Ga_2O_3," Appl. Phys. Lett. **115**(15), 152106 (2019).
[12] G.-ya Adachi and N. Imanaka, "The binary rare earth oxides," Chem. Rev. **98**(4), 1479–1514 (1998).
[13] R. H. Lamoreaux, D. L. Hildenbrand, and L. Brewer, "High-temperature vaporization behaviour of oxides II. Oxides of Be, Mg, Ca, Sr, Ba, B, Al, Ga, In, Ti, Si, Ge, Sn, Pb, Zn, Cd and Hg," J. Phys. Chem. Ref. Data **16**, 419 (1987).
[14] O. Bierwagen, A. Proessdorf, M. Niehle, F. Grosse, A. Trampert, and M. Klingsporn, "Oxygen-deficient oxide growth by subliming the oxide source material: The cause of silicide formation in rare earth oxides on silicon," Cryst. Growth Des. **13**(8), 3645–3650 (2013).
[15] H. J. Osten, E. Bugiel, M. Czernohorsky, Z. Elassar, O. Kirfel, and A. Fissel, "Molecular beam epitaxy of rare-earth oxides," Top. Appl. Phys. **106**, 101–114 (2007).
[16] M. Passlack, E. F. Schubert, W. S. Hobson, M. Hong, N. Moriya, S. N. G. Chu, K. Konstadinidis, J. P. Mannaerts, M. L. Schnoes, and G. J. Zydzik, "Ga_2O_3 films for electronic and optoelectronic applications," J. Appl. Phys. **77**(2), 686–693 (1995).
[17] R. Droopad, K. Rajagopalan, J. Abrokwah, L. Adams, N. England, D. Uebelhoer, P. Fejes, P. Zurcher, and M. Passlack, "Development of GaAs-based MOSFET using molecular beam epitaxy," J. Cryst. Growth **301–302**, 139–144 (2007).
[18] H. Paik, Z. Chen, E. Lochocki, A. Seidner H., A. Verma, N. Tanen, J. Park, M. Uchida, S. Shang, B.-C. Zhou, M. Brützam, R. Uecker, Z.-K. Liu, D. Jena, K. M. Shen, D. A. Muller, and D. G. Schlom, "Adsorption-controlled growth of La-doped $BaSnO_3$ by molecular-beam epitaxy," APL Mater. **5**(11), 116107 (2017).
[19] N. G. Combs, W. Wu, and S. Stemmer, "Stoichiometry control in molecular beam epitaxy of $BaSnO_3$," Phys. Rev. Mater. **4**(1), 014604 (2020).
[20] S. Ghose, M. S. Rahman, J. S. Rojas-Ramirez, S. Juan, M. Caro, R. Droopad, A. Arias, and N. Nedev, "Structural and optical properties of β-Ga_2O_3 thin films grown by plasma-assisted molecular beam epitaxy," J. Vac. Sci. Technol., B **34**(2), 02L109 (2016).
[21] A. B. Mei, L. Miao, M. J. Wahila, G. Khalsa, Z. Wang, M. Barone, N. J. Schreiber, L. E. Noskin, H. Paik, T. E. Tiwald, Q. Zheng, R. T. Haasch, D. G. Sangiovanni, L. F. J. Piper, and D. G. Schlom, "Adsorption-controlled growth and properties of epitaxial SnO films," Phys. Rev. Mater. **3**(10), 105202 (2019).
[22] S. Ghose, S. Rahman, L. Hong, J. S. Rojas-Ramirez, H. Jin, K. Park, R. Klie, and R. Droopad, "Growth and characterization of β-Ga_2O_3 thin films by molecular beam epitaxy for deep-UV photodetectors," J. Appl. Phys. **122**(9), 095302 (2017).
[23] P. Vogt and O. Bierwagen, "Comparison of the growth kinetics of In_2O_3 and Ga_2O_3 and their suboxide desorption during plasma-assisted molecular beam epitaxy," Appl. Phys. Lett. **109**(6), 062103 (2016).
[24] P. Vogt and O. Bierwagen, "Reaction kinetics and growth window for plasma-assisted molecular beam epitaxy of Ga_2O_3: Incorporation of Ga vs Ga_2O desorption," Appl. Phys. Lett. **108**(7), 072101 (2016).
[25] P. Vogt and O. Bierwagen, "Quantitative subcompound-mediated reaction model for the molecular beam epitaxy of III-VI and IV-VI thin films: Applied to Ga_2O_3," Phys. Rev. Mater. **2**(12), 120401 (2018).
[26] C. W. Bale, E. Bélisle, P. Chartrand, S. A. Decterov, G. Eriksson, A. E. Gheribi, K. Hack, I.-H. Jung, Y.-B. Kang, J. Melançon, A. D. Pelton, S. Petersen, C. Robelin,

J. Sangster, P. Spencer, and M.-A. Van Ende, "Reprint of: FactSage thermochemical software and databases, 2010-2016," Calphad **55**(4), 1–19 (2016).
[27]A. A. Radzig and B. M. Smirnov, *Reference Data on Atoms, Molecules, and Ions* (Springer, 1985), pp. 1–474.
[28]G. DeMaria, J. Drowart, and M. G. Inghram, "Thermodynamic study of InSb with a mass spectrometer," J. Chem. Phys. **31**(4), 1076–1081 (1959).
[29]R. Colin, J. Drowart, and G. Verhagen, "Mass-Spectrometric study of the vaporization of tin oxides," Trans. Faraday Soc. **61**, 1364–1371 (1965).
[30]E. Zimmermann, S. Königs, and D. Neuschiitz, "Determination by mass spectrometry of the partial pressures of SnO, Sn_2O_2, and Sn_6O_6 in equilibrium with oxygen saturated tin melts," Z. Phys. Chem. **193**(1–2), 195–206 (1996).
[31]R. P. Burns, "Systematics of the evaporation coefficient Al_2O_3, Ga_2O_3, In_2O_3," J. Chem. Phys. **44**(9), 3307–3319 (1966).
[32]P. Burns, "The effect of multiple binding states on the kinetics and mechanism of gas-surface interactions: $Ga_2O(g)$ + $Al_2O_3(s)$," Surf. Sci. **72**, 449–466 (1978).
[33]G. Balducci, G. Gigli, and G. Meloni, "Dissociation energies of the Ga_2, In_2, and GaIn molecules," J. Chem. Phys. **109**(11), 4384–4388 (1998).
[34]K. Zhou, S. K. Roy, and C. B. Zhao, "Ga_xO (x = 2–4) contain novel linear dicoordinate, T-shape tricoordinate and planar tetracoordinate oxygen," Russ. J. Inorg. Chem. **64**(3), 303–307 (2019).
[35]S. Gowtham, A. Costales, and R. Pandey, "Theoretical study of neutral and ionic states of small clusters of Ga_mO_n (m, n = 1, 2)," J. Phys. Chem. B **108**(45), 17295–17300 (2004).
[36]K. M. Maloney and D. A. Lynch, Int. J. Mass Spectrom. Ion Phys. **14**, 415–434 (1974).
[37]C. J. Frosch and C. D. Thurmond, "The pressure of Ga_2O over gallium-Ga_2O_3 mixtures," J. Phys. Chem. **66**(5), 877–878 (1962).
[38]H. Paik, private communication (2020).
[39]N. G. Combs, private communication (2020).
[40]M. E. White, M. Y. Tsai, F. Wu, and J. S. Speck, "Plasma-assisted molecular beam epitaxy and characterization of SnO_2(101) on r-plane sapphire," J. Vac. Sci. Technol., A **26**(5), 1300–1307 (2008).
[41]C. E. Simion, F. Schipani, A. Papadogianni, A. Stanoiu, M. Budde, A. Oprea, U. Weimar, O. Bierwagen, and N. Barsan, "Conductance model for single-crystalline/compact metal oxide gas-sensing layers in the nondegenerate limit: Example of epitaxial SnO_2 (101)," ACS Sens. **4**(9), 2420–2428 (2019).